THE PROCEEDINGS OF

AM-FPD 26

THE THIRTY-THIRD INTERNATIONAL WORKSHOP ON

ACTIVE-MATRIX FLATPANEL DISPLAYS AND DEVICES

－TFT Technologies and FPD Materials－

July 7 - 10, 2026

Ryukoku University Fukakusa Campus Jojukan, Japan

Next-Generation Thin-Film Electronics: Emerging Material, Functional Device, and Energy-Efficient Technology

Manvendra Chauhan and Satinder K. Sharma*

School of Computing and Electrical Engineering (SCEE), Indian Institute of Technology (IIT), Mandi, MANDI-175005, Himachal Pradesh, India.

E-mail: satinder@iitmandi.ac.in*

The development of energy-efficient electronic and optoelectronic systems increasingly depends on advances in thin-film materials, interface engineering, and scalable device architectures. In this work, a lead-free hybrid perovskite-based resistive random-access memory (ReRAM) device is presented as a representative thin-film electronic platform for low-voltage and optically tunable switching. The device employs a PEAI-passivated triple-cation europium (Eu)-based perovskite switching layer (SL) integrated in Ag/PEAI/CsMAFAEuI$_3$/FTO structures. The use of Cs/MA/FA compositional engineering and Eu-based perovskite chemistry provides a promising route toward environmentally compatible memory devices, while PEAI surface passivation helps suppress grain-boundary defects, reduce leakage pathways, and improve device stability. To the best of our knowledge, this work represents one of the first demonstrations of PEAI-passivated lead-free Eu-based triple-cation perovskite ReRAM exhibiting optically tunable low-voltage switching and energy-efficient behaviours. Optical, morphological, and structural analyses show that PEAI treatment at 90 °C enhances film quality, smoothens the surface morphology, introduces quasi-2D surface ordering, and reduces microstrain while retaining the 3D perovskite framework. The fabricated device exhibits photo-tunable bipolar resistive switching (RS) with reduced operating voltage under white-light illumination compared with dark operation. The fabricated ReRAM devices exhibited a ~ 14.3% reduction in operating voltages (SET/RESET) compared with operation under dark conditions. Under white-light illumination, the ReRAM device exhibited ~ 1.25-fold (~25%) increase in the memory window compared with operation in the dark. These findings demonstrate that surface-engineered lead-free perovskites constitute a promising, scalable thin-film electronic platform for future low-power memory, neuromorphic hardware, and sustainable computing technologies.

1. Introduction

The rapid proliferation of artificial intelligence, the Internet of Things (IoT), wearable electronics, and edge computing has generated strong demand for next-generation non-volatile memory technologies that feature energy-efficient operation, low power consumption, high scalability, and compatibility with standard scalable thin-film processing. Conventional silicon-based memories face increasing challenges associated with scaling limitations and energy dissipation. Hybrid halide perovskites (HHPs) have emerged as promising switching materials for non-volatile memory because they combine solution-processability, strong ionic-electronic coupling, a defect-tolerant electronic structure, a simple metal-insulator-metal architecture, low operating voltage, and potential integration into neuromorphic computing systems. Within this family, triple-cation perovskites containing Cs^+, methylammonium (MA^+), and formamidinium (FA^+) are particularly attractive because compositional engineering can improve phase stability, suppress trap-rich disorder, and sharpen electronic transitions[1)-4)]. The smaller ionic radius of Cs^+ (~1.67 A) [1)], compared with FA^+ (~2.53 A) [5)] and MA^+ (~2.17 A) [6)], can slightly contract and stabilise the lattice, thereby supporting more reproducible RS.

Most reported perovskite ReRAM devices still rely on Pb-containing compounds, raising concerns over toxicity and long-term environmental compatibility. Consequently, the development of environmentally benign and lead-free perovskite memories has become increasingly important for sustainable electronics and green semiconductor technologies. Sn^{2+} and Bi^{3+} have been explored as lead-free alternatives; however, Sn^{2+} is susceptible to oxidation into Sn^{4+}, which introduces deep trap states [7),8)], while Bi^{3+} often favours low-dimensional defect-rich frameworks that restrict uniform conduction [9),10)]. Eu^{2+} offers a reliable lead-free route due to its divalent character, a favourable octahedral ionic radius (~1.26 A) [5)], and potential compatibility with the B-site of a 3D iodide perovskite lattice. In addition, the optically active nature of Eu-based halide systems is useful for photo-responsive memory operation.

Despite these advantages, perovskite ReRAM reliability is frequently limited by uncontrolled filament growth, grain-boundary-assisted ion migration, and surface defect states. These factors increase leakage in the high-resistance state (HRS), destabilise the low-resistance state (LRS), and narrow the memory window. Surface passivation using organic spacer cations such as phenylethylammonium iodide (PEAI) can form a quasi-2D capping layer over the perovskite surface [11),12)]. Such passivation has been reported to enhance crystallinity, reduce trap-mediated losses, and

ISBN 978-4-9914654-0-6 ©2026 FTFMD

improve operational stability [12)–14)]. Although PEAI passivation has been extensively investigated in photovoltaic devices, its influence on optically tunable lead-free Eu-based perovskite ReRAM remains largely unexplored. Therefore, systematic investigation of the role of PEAI-induced surface/interface engineering on defect suppression, structural ordering, and photo-assisted resistive switching is essential. Here, we present a compact study of PEAI-passivated $CsMAFAEuI_3$ ReRAM devices with the Ag/PEAI/$CsMAFAEuI_3$/FTO structure, emphasising low-voltage, optically tunable RS.

2. Experimental Method

The $CsMAFAEuI_3$ SL was prepared through a solution-processed route under an inert argon atmosphere. Methylammonium iodide (MAI, 1.3 mM) and europium(II) iodide (EuI_2, 1.14 mM) were dissolved in a DMF:DMSO mixture (9:1 v/v) and stirred at 50 °C for 2 h to obtain the $MAEuI_3$ precursor. A separate FAI solution (1.3 mM) was prepared in the same solvent system and added at 10 v/v% to form $MAFAEuI_3$. A CsI solution (1.3 mM) was then introduced at 15 v/v%, yielding the optimised $CsMAFAEuI_3$ formulation, denoted CsI-15.

FTO-coated glass substrates were sequentially cleaned by sonication in deionised water, acetone, and isopropyl alcohol for 15 min each, followed by a UV/O_3 treatment for 30 min. The perovskite precursor was spin-coated onto cleaned FTO substrates (**Fig. 1a**), followed by toluene antisolvent treatment during spinning and annealing at 120 °C for 30 min (**Fig. 1b**). The resulting HHP film thickness was ~ 270 nm. PEAI was dissolved in isopropyl alcohol at 50 °C (**Fig. 1c**) and spin-coated on the optimised CsI-15 thin film (**Fig. 1d**), followed by annealing at 60 °C, 90 °C, or 120 °C (**Fig. 1e**) to identify the most effective passivation condition. The PEAI-passivated film thickness was measured to be ~123 nm. Ag top electrodes (~60 nm) were thermally evaporated through a shadow mask, defining an active device area of 0.0025 cm^2.

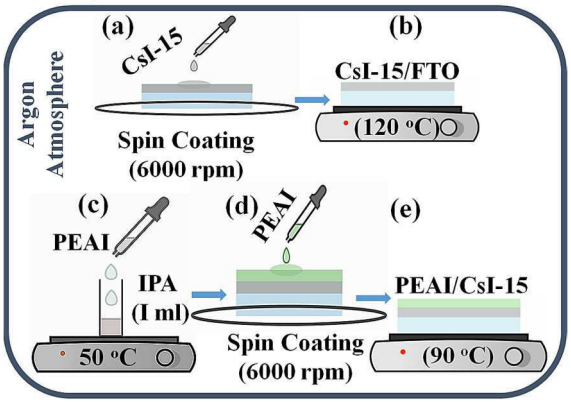

Fig. 1. Schematic thin-film processing: (a) CsI-15 perovskite spin coating, (b) CsI-15 thin film annealing, (c) PEAI precursor formulation, (d) PEAI passivation over CsI-15 thin film through spin coating, and (e) PEAI/CsI-15 stack annealing, under an argon atmosphere.

3. Results and Discussion

As shown in **Fig. 2a**, the CsI-15 thin film exhibits a clear optical absorption response, confirming the formation of the perovskite SL. After PEAI surface passivation, the optical response changes noticeably, as shown in **Fig. 2b**. Among the investigated annealing temperatures, the PEAI-treated film annealed at 90 °C shows the highest absorbance and the sharpest absorption onset, indicating more effective surface defect suppression and improved film quality. The 60 °C sample showed weaker absorption and a broad edge, consistent with incomplete passivation, while the 120 °C sample showed slight red-shifting (**Fig. 2b**) and broadening that may be associated with partial degradation or volatilisation of organic components. These observations support 90 °C as the preferred PEAI annealing condition. The enhanced optical absorption and sharper absorption edge observed after PEAI treatment suggest reduced trap-assisted recombination and improved electronic coupling, which are expected to facilitate efficient carrier transport during resistive switching.

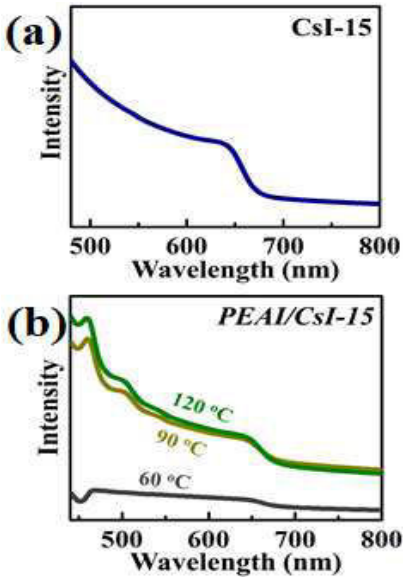

Fig. 2. (a) UV-vis absorption spectra of CsI-15 film and (b) PEAI-passivated CsI-15 films annealed at 60, 90, and 120 °C

FESEM analysis shown in **Fig 3** further confirmed the passivation effect. The pristine CsI-15 film showed distinct grains and visible grain boundaries (**Fig. 3a**), which can serve as trap-rich leakage paths and Ag^+ migration channels. After PEAI treatment, the surface became smoother and more compact (**Fig. 3b**), with strongly suppressed grain-boundary contrast. This morphological change is important for ReRAM operation because a more uniform interface can limit uncontrolled filament growth and reduce HRS leakage. The smoother, denser morphology achieved after PEAI treatment is expected to suppress localised electric-field concentration and uncontrolled conductive filament formation, thereby improving switching uniformity and device reliability.

ISBN 978-4-9914654-0-6 ©2026 FTFMD

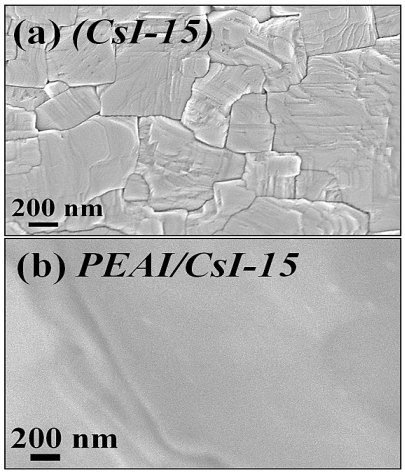

Fig. 3. FESEM surface morphology of CsI-15 films before and after PEAI passivation: (a) pristine film with visible grain boundaries and (b) PEAI-treated film showing a smoother, compact surface morphology.

XRD patterns shown in **Fig. 4a** revealed that PEAI passivation at 90 °C introduced low-angle reflections at ~ 5.3°, 10.6°, and 15.9° (2θ), consistent with quasi-2D Ruddlesden-Popper-like ordering associated with PEA^+ at the surface or grain-boundary regions [11),15),16)].

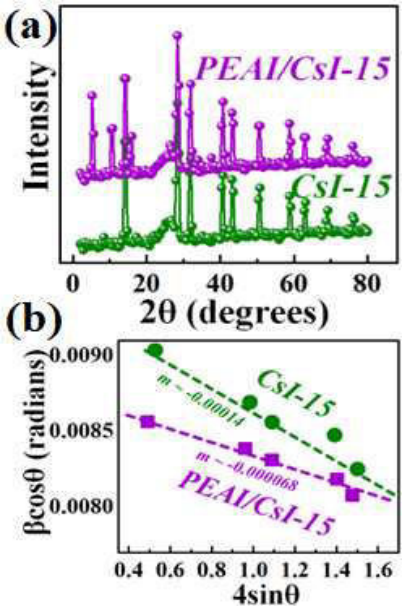

Fig. 4. (a) XRD and (b) Williamson–Hall analysis of $CsMAFAEuI_3$ films before and after PEAI passivation

At the same time, the main 3D perovskite reflections at ~14.2° (110), ~28.45° (220), ~31.9° (310), ~40.7° (400), and ~43.3° (330) were retained, indicating that PEAI modifies the surface/interface without destroying the underlying 3D lattice. W-H analysis (**Fig. 4b**) showed a reduction in compressive microstrain from ~ -3.50×10^{-5} before passivation to -1.7×10^{-5} after PEAI treatment, corresponding to a ~ 2.05 fold reduction in strain magnitude. This reduction is consistent with improved lattice coherence and lower defect density.

The Ag/PEAI/CsI-15/FTO devices exhibited bipolar RS under both dark and white-light conditions. As shown in **Fig. 5a**, the SET voltage was ~ 0.28 V in the dark and ~ 0.24 V under white-light illumination, while the RESET voltage was - 0.28 V and - 0.24 V, respectively. The modest reduction in switching voltage under illumination indicates optically assisted carrier generation and easier modulation of the conductive pathway. The device showed a high switching contrast, with LRS/HRS ratios of ~ 7.77×10^4 in the dark and ~ 9.71×10^4 under white-light excitation.

Endurance measurements up to 10000 cycles showed stable, well-separated resistance states up to ~ 9500 cycles under both dark and illuminated operation (**Fig. 5b**). Beyond this point, HRS leakage increased abruptly, marking the onset of endurance failure. Under dark operation, the median HRS current increased from 4.10×10^{-7} A cm^{-2} before failure to 2.43×10^{-4} A cm^{-2} during 9600-10000 cycles, corresponding to an increase of ~ 593 times.

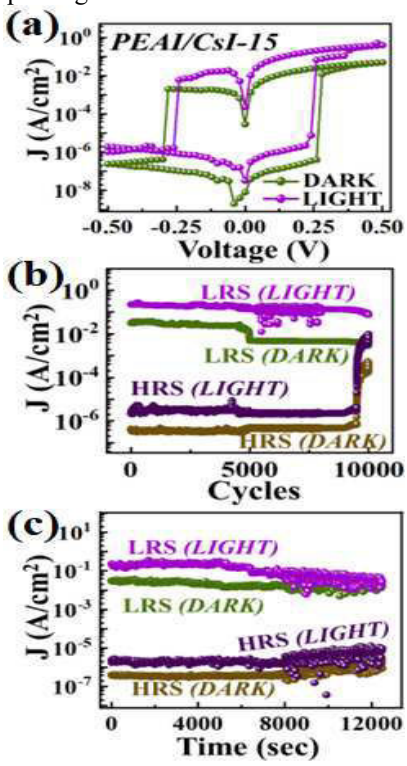

Fig. 5. (a) Low-voltage bipolar RS, (b) endurance, and (c) retention characteristics of Ag/PEAI/CsI-15/FTO ReRAM devices measured under dark and white-light illumination.

Under illumination, the HRS current increased from 2.61×10^{-6} A cm^{-2} to 4.26×10^{-3} A cm^{-2}, corresponding to an increase of ~ 1630 times. The memory window consequently collapsed from the 10^4-10^5 range during stable operation to about 10 by the end of cycling. The degradation in endurance performance during prolonged cycling is primarily attributed to cumulative defect generation, residual conductive filament fragments, and progressive degradation of the PEAI/perovskite interface.

Retention measurements showed data stability up to 12491 s,

ISBN 978-4-9914654-0-6 ©2026 FTFMD

although fluctuations became more pronounced after ~ 7480 s (**Fig. 5c**). This behaviour suggests that PEAI passivation substantially improves the device stability, but the HRS remains the more vulnerable state during extended operation. Overall, the improved switching contrast, low operating voltage, and optically tunable response can be attributed to the combined effects of Cs-assisted lattice stabilisation, Eu-based lead-free perovskite composition, and PEAI-mediated surface/interface passivation.

4. Conclusions

PEAI-passivated lead-free triple-cation $CsMAFAEuI_3$ (CSI-15) perovskite SL was integrated into Ag/PEAI/CsI-15/FTO ReRAM devices and evaluated under dark and white-light conditions. PEAI treatment at 90 °C improved optical absorption, smoothed the film surface, introduced quasi-2D surface ordering, and reduced the W-H microstrain magnitude from ~ -3.50×10^{-5} to ~ -1.7×10^{-5} while preserving the 3D perovskite framework. The devices achieved low SET/RESET voltages of ±0.28 V in the dark and ±0.24 V under white light, with LRS/HRS ratios approaching 10^5. Stable switching was maintained up to ~ 9.5×10^3 cycles, with retention measured up to 12491 s. These results indicate that PEAI-passivated Eu-based triple-cation perovskites are promising for low-voltage, optically tunable, lead-free ReRAM, although further optimisation is required to suppress late-cycle HRS leakage and improve long-term retention stability.

Acknowledgments

The authors sincerely acknowledge the C4DFED facility at IIT Mandi for providing access to the Class 100 cleanroom and associated facilities used for device fabrication, FESEM-based nanoscale imaging, and electrical characterisation. The authors also thank the Advanced Materials Research Centre (AMRC) at IIT Mandi for its support with chemical characterisation.

References

1) S. M. Lee, H. Kim, D. H. Kim, W. Bin Kim, J. M. Lee, J. Choi, H. Shin, G. S. Han, H. W. Jang and H. S. Jung, ACS Appl. Mater. Interfaces 12 [14], 17039 (2020).
2) M. Othman, Q. Jeangros, D. A. Jacobs, M. H. Futscher, S. Zeiske, A. Armin, A. Jaffrès, A. G. Kuba, D. Chernyshov, S. Jenatsch, S. Züfle, B. Ruhstaller, S. Tabean, T. Wirtz, S. Eswara, J. Zhao, T. J. Savenije, C. Ballif, C. M. Wolff and A. Hessler-Wyser, Energy Environ. Sci. 17 [11], 3832 (2024).
3) M. Saliba, T. Matsui, J. Y. Seo, K. Domanski, J. P. Correa-Baena, M. K. Nazeeruddin, S. M. Zakeeruddin, W. Tress, A. Abate, A. Hagfeldt and M. Grätzel, Energy Environ. Sci. 9 [6], 1989 (2016).
4) F. Alam, K. D. Wegner, S. Pouget, L. Amidani, K. Kvashnina, D. Aldakov and P. Reiss, Journal of Chemical Physics [DOI:10.1063/1.5126473].
5) R. D. Shannon, Foundations of Crystallography 32 [5], 751 (1976).
6) G. Kieslich, S. Sun and A. K. Cheetham, Chem. Sci. 6 [6], 3430 (2015).
7) T. Wu, X. Liu, X. Luo, X. Lin, D. Cui, Y. Wang, H. Segawa, Y. Zhang and L. Han, Joule 5 [4], 863 (2021).
8) E. Aktas, N. Rajamanickam, J. Pascual, S. Hu, M. H. Aldamasy, D. Di Girolamo, W. Li, G. Nasti, E. Martínez-Ferrero, A. Wakamiya, E. Palomares and A. Abate, Commun. Mater. 3 [1], 104 (2022).
9) X. Chen, M. Jia, W. Xu, G. Pan, J. Zhu, Y. Tian, D. Wu, X. Li and Z. Shi, Adv. Opt. Mater. 11 [3], 2202153 (2023).
10) A. J. Lehner, D. H. Fabini, H. A. Evans, C. A. Hébert, S. R. Smock, J. Hu, H. Wang, J. W. Zwanziger, M. L. Chabinyc and R. Seshadri, Chemistry of Materials 27 [20], 7137 (2015).
11) A. A. Sutanto, R. Szostak, N. Drigo, V. I. E. Queloz, P. E. Marchezi, J. C. Germino, H. C. N. Tolentino, M. K. Nazeeruddin, A. F. Nogueira and G. Grancini, Nano Lett. 20 [5], 3992 (2020).
12) C. Zhi, Z. Li and B. Wei, APL Mater. [DOI:10.1063/5.0056106].
13) J. Liu, J. Gong, H. Wei, Y. Li, H. Wu, C. Jiang, Y. Li and W. Xu, Nat. Commun. 13 [1], 7427 (2022).
14) G. Wu, R. Liang, M. Ge, G. Sun, Y. Zhang and G. Xing, Advanced Materials 34 [8], 2105635 (2022).
15) M. C. Tang, S. Zhang, T. J. Magnanelli, N. V. Nguyen, E. J. Heilweil, T. D. Anthopoulos and C. A. Hacker, Mater. Adv. 2 [4], 1253 (2021).
16) F. Fiorentino, M. D. Albaqami, I. Poli and A. Petrozza, ACS Appl. Mater. Interfaces 14 [30], 34180 (2022).

ISBN 978-4-9914654-0-6 ©2026 FTFMD